

 Open access • Journal Article • DOI:10.1088/1361-6463/AAAE7A

## Atomic scale simulation of H<sub>2</sub>O<sub>2</sub> permeation through aquaporin: toward the understanding of plasma cancer treatment — [Source link](#)

Maksudbek Yusupov, Dayun Yan, Rodrigo M. Cordeiro, Annemie Bogaerts

**Institutions:** University of Antwerp, George Washington University, Universidade Federal do ABC

**Published on:** 28 Feb 2018 - Journal of Physics D (IOP Publishing)

Related papers:

- [Effect of lipid peroxidation on membrane permeability of cancer and normal cells subjected to oxidative stress](#)
- [Toward understanding the selective anticancer capacity of cold atmospheric plasma—A model based on aquaporins \(Review\)](#)
- [Cold atmospheric plasma, a novel promising anti-cancer treatment modality.](#)
- [Hampering Effect of Cholesterol on the Permeation of Reactive Oxygen Species through Phospholipids Bilayer: Possible Explanation for Plasma Cancer Selectivity.](#)
- [The role of aquaporins in the anti-glioblastoma capacity of the cold plasma-stimulated medium](#)

Share this paper:    

View more about this paper here: <https://typeset.io/papers/atomic-scale-simulation-of-h2o2-permeation-through-aquaporin-3v9allja3r>

**This item is the archived peer-reviewed author-version of:**

Atomic scale simulation of  $H_2O_2$  permeation through aquaporin : toward the understanding of plasma cancer treatment

**Reference:**

Yusupov Maksudbek, Yan Dayun, Cordeiro Rodrigo M., Bogaerts Annemie.- Atomic scale simulation of  $H_2O_2$  permeation through aquaporin : toward the understanding of plasma cancer treatment  
Journal of physics: D: applied physics - ISSN 0022-3727 - 51:12(2018), 125401  
Full text (Publisher's DOI): <https://doi.org/10.1088/1361-6463/AAAE7A>  
To cite this reference: <https://hdl.handle.net/10067/1493820151162165141>

# Atomic scale simulation of H<sub>2</sub>O<sub>2</sub> permeation through aquaporin: toward the understanding of plasma-cancer treatment

Maksudbek Yusupov<sup>\*1</sup>, Dayun Yan<sup>2</sup>, Rodrigo M. Cordeiro<sup>3</sup> and Annemie Bogaerts<sup>1</sup>

<sup>1</sup> Research Group PLASMANT, Department of Chemistry, University of Antwerp, Universiteitsplein 1, B-2610 Antwerp, Belgium

<sup>2</sup> The Micro-propulsion and Nanotechnology Laboratory, Department of Mechanical and Aerospace Engineering, The George Washington University, Science & Engineering Hall, 800 22<sup>nd</sup> Street, NW, Room 3550, Washington, DC 20052, USA

<sup>3</sup> Centro de Ciências Naturais e Humanas, Universidade Federal do ABC, Avenida dos Estados 5001, CEP 09210-580, Santo André, SP, Brazil

E-mail: maksudbek.yusupov@uantwerpen.be

## Abstract

Experiments have demonstrated the potential selective anticancer capacity of cold atmospheric plasmas (CAPs), but the underlying mechanisms remain unclear. Using computer simulations, we try to shed light on the mechanism of selectivity, based on aquaporins (AQPs), i.e., transmembrane protein channels transferring external H<sub>2</sub>O<sub>2</sub> and other reactive oxygen species, created e.g. by CAPs, to the cell interior.

Specifically, we perform molecular dynamics simulations for the permeation of H<sub>2</sub>O<sub>2</sub> through AQP1 (one of the members of the AQP family) and the palmitoyl-oleoyl-phosphatidylcholine (POPC) phospholipid bilayer (PLB). The free energy barrier of H<sub>2</sub>O<sub>2</sub> across AQP1 is lower than for the POPC PLB, while the permeability coefficient, calculated using the free energy and diffusion rate profiles, is two orders of magnitude higher. This indicates that the delivery of H<sub>2</sub>O<sub>2</sub> into the cell interior should be through AQP.

Our study gives a better insight into the role of AQPs in the selectivity of CAP for treating cancer cells.

## 1. Introduction

Cold atmospheric plasmas (CAPs) are increasingly gaining attention for cancer treatment [1-11]. They cause more cell death or growth inhibition on cancer cells than on homologous normal cells under the same experimental conditions *in vitro* [6, 12-14]. The risk assessment on multiple cell lines demonstrated no mutagenic potential up to at least 180 seconds of CAP treatment, which generated 50  $\mu$ M of H<sub>2</sub>O<sub>2</sub> in the CAP treated solution [5].

Understanding the selective anti-cancer capacity of CAP treatment is a key challenge [3]. It is linked to the selective rise of intracellular reactive oxygen species (ROS) in CAP-treated cancer cells [15-19]. Several explanations were proposed to reveal the underlying mechanism. The earliest explanation attributed the selectivity to the different basal intracellular ROS levels between cancer and normal cells [20, 21]. Due to some intrinsic factors (e.g., aberrant metabolism for some cancer types, mitochondrial dysfunction and loss of functional p53), the basal intracellular ROS levels in some cancer cells may be higher than in normal cells [22, 23]. When further extracellular ROS stress is exerted on them, the intracellular ROS level in these cancer cells may pass a threshold, leading to cell death [20, 21]. Thus, these cancer cells may experience more ROS-caused apoptosis and other ROS-caused cellular damage than some normal cells upon CAP treatment, according to literature [6].

However, this model cannot explain the selective rise of intracellular ROS in cancer cells rather than in normal cells [15-19]. Therefore, recent molecular dynamics (MD) simulations provide another explanation based on the potential different trends to form membrane pores in

the cytoplasmic membrane. They reveal that lipid oxidation in the phospholipid bilayer (PLB) yields an increase of the bilayer permeability to extracellular ROS [24, 25] and a drop of the electric field threshold for membrane pore formation, which may facilitate extracellular ROS penetration [25]. Even without electric field, MD simulations reveal that pores can be formed when all phospholipids (PLs) are oxidized [26]. Furthermore, a significant effect of cholesterol on the ROS permeation across the PLB was demonstrated. A higher cholesterol fraction increases the order of the PLB and the transfer free energy barrier height and width. Moreover, it forms a local free energy minimum in the membrane center, and creates extra free energy barriers [26, 27]. Cholesterol may thus be able to protect the membrane against pore formation upon lipid peroxidation [26-28]. Some cancer cells, like leukemic cells, have a lower cholesterol/PL ratio compared with normal counterparts such as lymphocytes [29]. Thus, the CAP-originated ROS and reactive nitrogen species (RNS) may enter cancer cells more easily compared with normal cells, based on the tendency to form pores in the cytoplasmic membrane.

Another model proposed recently is about the different expression levels of membrane channels for ROS (mainly  $H_2O_2$ ) in cancer cells and normal cells. Cancer biology research confirms that most cancer tissues express more aquaporins (AQPs) in their cytoplasmic membranes than homologous normal tissues [30]. AQPs are small transmembrane channels, mainly for  $H_2O$  but also for other small molecules like  $H_2O_2$ , NO, and  $NO_3^-$  [30-35].  $H_2O_2$  is a necessary component for the anti-cancer capacity of CAP-stimulated solutions and direct CAP treatment [36-42]. Although  $H_2O_2$  alone cannot explain the whole selective anti-cancer mechanism of CAP-stimulated solutions [42-45], it has shown its selective anti-cancer capacity over some cancer cell lines, such as lymphoma cells [46]. Recently, knocking out AQP8 in glioblastoma cells could significantly weaken the toxicity of CAP-stimulated medium on these cells [47]. This was the first evidence for the role of membrane channel proteins in plasma medicine. Furthermore, the uptake of  $H_2O_2$  in colon adenocarcinoma HT29 cells, mammalian HEK 293 cells and cervical cancer HeLa cells can be drastically increased by the expression of AQP3 on these cells [48]. Based on these clues, we speculate that  $H_2O_2$  produced by CAP may diffuse into cancer cells significantly faster than into homologous normal cells through AQPs [6]. Such transmembrane diffusion differences may cause more intracellular ROS, and thus cellular damage and apoptosis in cancer cells than in normal cells [6]. So far, AQP1, 3, 8 and 9 have been confirmed as the membrane channels of  $H_2O_2$  [48-50]. AQP1 is widely expressed in cancerous tissues, including astrocytoma, breast cancer, cervical cancer, colorectal cancer, lung cancer, and ovarian cancer [6]. Thus, studying the role of AQP1 in the anti-cancer capacity of CAP provides clues to several studies in plasma medicine. Moreover, it will also be of great interest to other cancer therapies producing  $H_2O_2$  (or ROS in general), such as chemotherapy, radiotherapy and photodynamic therapy.

Based on these considerations, we investigate here the permeation of  $H_2O_2$  across both AQP1 and the PLB, to determine the precise role of AQPs in the selective anti-cancer capacity of CAP. For this purpose, we perform MD simulations. Specifically, we calculate the free energy and diffusion rate profiles of  $H_2O_2$ , which allows to determine the permeability coefficient of  $H_2O_2$  through AQP1 and the PLB. Comparison of the latter enables us to define whether the delivery of ROS into the cell interior is accomplished through AQPs or the PLB. Thus, the performed simulations will give more insight in this proposed mechanism based on AQPs for the selectivity of CAP treatment towards cancer cells.

It should be mentioned that the transport of  $H_2O_2$  in and out of the cell facilitated by AQPs is well known in literature. However, there has been some controversy about the transport ability of different AQP isoforms. The first studies showed that the heterologous expression of human AQP1 had no effect on yeast cell viability in the presence of  $H_2O_2$  [51]. More recent studies proposed that the lack of  $H_2O_2$  transport in AQP1 could be rather related to low expression levels [49]. In fact, moderate  $H_2O_2$  permeability was detected in rat AQP1. Our results add up to previous computational studies [33] that support the role of AQP1 in  $H_2O_2$  transport. Plasma

medicine might benefit from future studies of the structural determinants of  $\text{H}_2\text{O}_2$  conductivity by AQPs.

## 2. Computational details

We carried out MD simulations to study the permeation of  $\text{H}_2\text{O}_2$  across the AQP1 transmembrane protein as well as the PLB. The latter was used as a simple model system for the cell membrane. Specifically, we calculated the free energy and diffusion rate profiles, as well as the permeability coefficients, of  $\text{H}_2\text{O}_2$  in order to elucidate which of these structures is most favorable for  $\text{H}_2\text{O}_2$  penetration to the cytoplasm. The model system for AQP1 consists of one AQP1 tetramer (crystal structure is available in the Protein Data Bank under the code 1J4N [52]) embedded in a 1-palmitoyl-2-oleoyl-*sn*-glycero-3-phosphocholine (POPC) PLB and covered with water layers on top and at the bottom, whereas the model system for the PLB is only composed of POPC lipids and water layers (see figure 1). Note that POPC was chosen because it is at the physiologically relevant fluid state at the temperature adopted in our MD simulations.

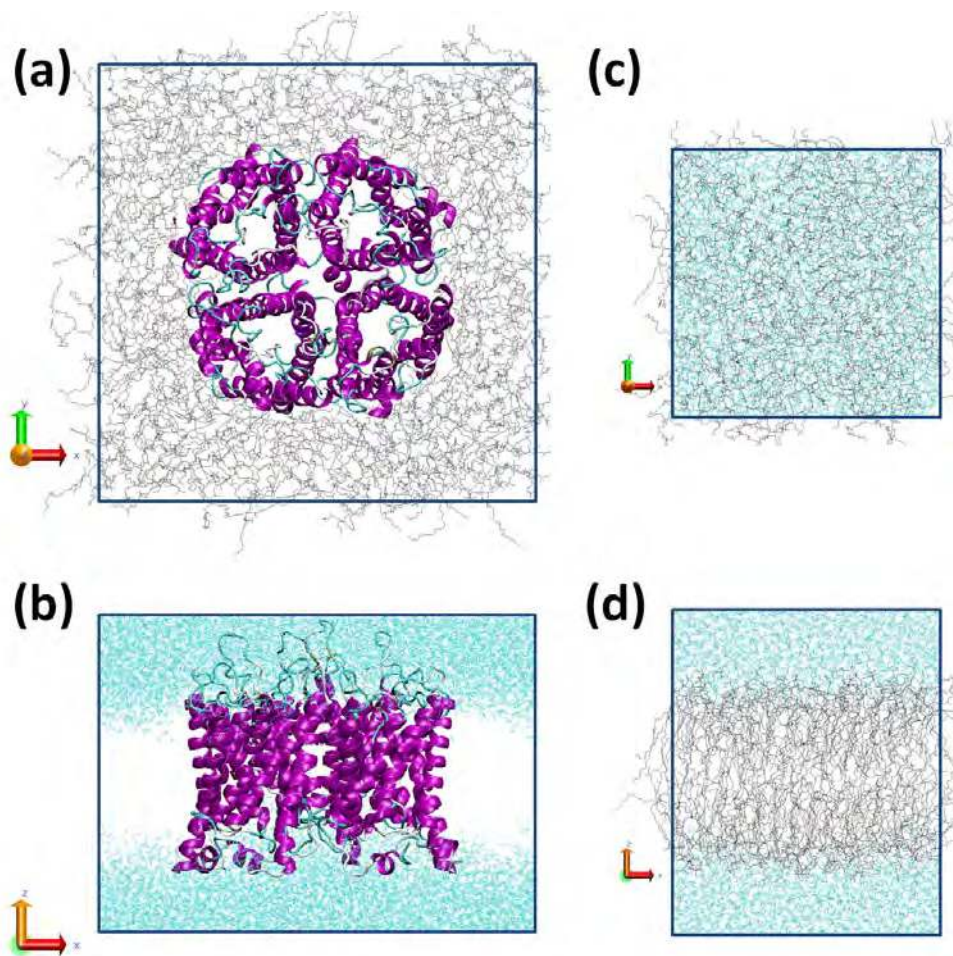


**Figure 1.** (a) Top and (b) side view of the AQP1 tetramer embedded in a POPC PLB (see gray color in (a)) and covered with water layers on top and at the bottom (see cyan color in (b)). For clarity, the POPC lipids are removed in (b) and the water layers are removed in (a). The tetramer gives rise to 4 pores (one for each monomer) as well as a central cavity. (c) Top and (d) side view of the POPC PLB. The POPC lipids and the water layers covering them at the top and bottom are shown in gray and cyan colors, respectively.

In general, AQPs are present in tetrameric form, where each monomer acts as an independent channel. Each monomer contains six tilted transmembrane  $\alpha$ -helices, of which two of them (i.e., re-entrant short helices) create a pathway for the permeation of water (or other small molecules, like  $\text{H}_2\text{O}_2$ ). Along the pore, a series of backbone carbonyl groups and hydrophilic side chains create a narrow water file and at the pore center two highly conserved Asn-Pro-Ala (NPA) motifs provide selectivity against the passage of ions [52, 53]. Another constriction region, so-called aromatic/Arg (ar/R), which is found close to the extracellular exit of the channel, also contributes to the selectivity (see figure 4(a,b) below). More information about AQP1 is given in [33].

We derived the model systems for AQP1 and the POPC PLB from [33] and [54], respectively, and more details about the preparation and equilibration of these systems are given there. Briefly, the initial configurations of these systems had their energy minimized using the steepest descent algorithm. Subsequently, the systems were equilibrated for  $\sim 100$  ns in the NPT-ensemble (i.e., constant number of particles, pressure and temperature) by applying the Nose-Hoover thermostat [55] and the semi-isotropic Parrinello-Rahman barostat [56]. The calculated root mean square displacements of the  $\text{C}_\alpha$  atoms of AQP1 showed that the chosen equilibration time was sufficient [33]. Note that this is a standard practice that allows to identify secondary structure deviations in proteins (see, e.g., [57]). In the case of the POPC PLB, the obtained average surface area per lipid, which defines typical properties of the bilayer, was closer to the experimental measurements reported in literature [54]. The applied reference temperature and pressure were 310 K and 1 atm, respectively. Periodic boundary conditions were applied in all Cartesian directions. In all simulations, a time step of 2 fs was used and the GROMOS54A7 force field parameters were employed for interatomic interactions [57] in combination with the SPC water model [58]. The parameters of  $\text{H}_2\text{O}_2$  species were adopted from [54]. For the electrostatic interactions, a 0.9 nm cut-off was applied, using the particle mesh Ewald method [59], whereas Lennard-Jones interactions were truncated using a twin-range cutoff at 0.9 and 1.4 nm.

All simulations were carried out using the GROMACS 4.6 package [60, 61]. The last 50 ns of the equilibration was used to extract the structures of the model systems to calculate the free energy, diffusion rate and permeability coefficient.

## 2.1 Free energy profiling

The free energy profiles of  $\text{H}_2\text{O}_2$  across both AQP1 and POPC PLB were obtained using umbrella sampling (US) simulations. For each energy profile, a certain number of US windows (i.e., 66 for AQP1 and 70 for the PLB) was defined along the structure normal ( $z$ -axis), which were separated by 1 Å. In this manner, the sampling windows spanned the entire system. Six (in the case of AQP1, see figure 2) or seven (in the case of the PLB) US windows, separated by 10 Å, were sampled simultaneously during each simulation to save computational resources.

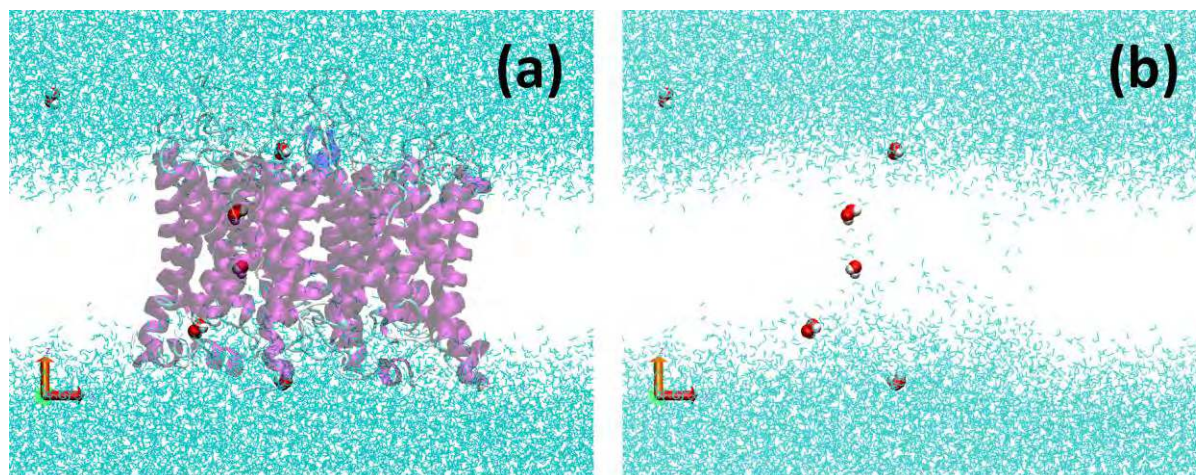


**Figure 2.** Snapshot from the MD simulation, where six  $\text{H}_2\text{O}_2$  molecules, separated by 10 Å in  $z$ -direction, are created for performing US calculations; the system with (a) and without (b) AQP1

tetramer. Water layers are shown in cyan color, the lipids are removed for the sake of clarity. The  $H_2O_2$  molecules (shown in red and white colors) can freely travel in the x- and y-directions (see the molecules on top and at the bottom water layers), whereas their motion is restricted in z. The motions of those  $H_2O_2$  molecules that are created inside the pore are restrained by the amino acids of the channel. It is clear that the  $H_2O_2$  molecules inside the pore are surrounded by waters (see (b)). This indicates that US simulations are performed in the hydrated pores of the AQP1.

Thus, eleven (in the case of AQP1) or ten (in the case of the PLB) US simulations were needed to obtain each energy profile. A harmonic bias with a force constant of  $2000 \text{ kJ.mol}^{-1}.\text{nm}^{-2}$  was applied along the z-direction on the  $H_2O_2$  molecules to restrict their motion, whereas they could freely travel in the x- and y-directions. Note that the created  $H_2O_2$  molecules inside the pores of AQP1 were surrounded by water molecules (see figure 2), which means that US simulations were performed in the hydrated pores of the AQP1. As mentioned above, during each US simulation the  $H_2O_2$  molecules were separated by  $10 \text{ \AA}$  along the z-direction in order to avoid long distance interactions between these molecules. With this condition, a 4 ns US MD simulation was performed, where during the last 2 ns the US histograms were collected. The conditions used in these simulations were identical to those used during the equilibration runs (see above). We used six structures derived from the last 50 ns equilibration run (i.e., at 0, 10, 20, 30, 40 and 50 ns) for both model systems, and for each structure we performed five sets of US simulations: each set was equal to 10 or 11 US MD, see above. Note that in the case of AQP1, these five sets of US simulations corresponded to the four pores and one central cavity. The latter was performed to check whether  $H_2O_2$  would be able to easily penetrate through the central cavity or not (see figure 6 below). Thus, the final free energy profiles were obtained by averaging over 24 energy profiles (i.e., 4 sets of US MD  $\times$  6 structures, if considering only the pores) in the case of AQP1 and 30 energy profiles (i.e., 5 sets of US MD  $\times$  6 structures) in the case of the PLB. These energy profiles differed from one another based on their starting structure, and therefore, averaging of them allowed us to obtain some statistical variations. Hence, in total  $264$  (for the AQP1 pores) +  $66$  (for the AQP1 central cavity) +  $300$  (for the POPC PLB) =  $630$  US simulations were performed to obtain the free energy profiles. All free energy profiles were constructed using the weighted histogram analysis method (WHAM) [62], as implemented in the *g\_wham* tool of GROMACS.

## 2.2 Diffusion rate profiling

The position-dependent diffusion coefficients of  $H_2O_2$  molecules across both AQP1 and the PLB were calculated using the so-called GLE method [63, 64], applying the same US MD simulations as performed for the free energy profiles (see above). This method is based on the solutions to the generalized Langevin equation (GLE) for a harmonic oscillator [64]. Through the integration of the position autocorrelation function (PACF), the diffusion coefficient of a solute in each z position  $D(z)$  is calculated as follows:

$$D(z_i = \langle z \rangle_i) = \frac{\text{var}(z)^2}{\tau} \quad (1)$$

$\tau$  is calculated from the integral of the PACF ( $C_z(t)$ ):

$$\tau = \int_0^\infty C_z(t) dt \quad (2)$$

The function  $C_z(t)$  can be calculated in a straightforward way by a summation over the trajectory [65]:

$$C_z(t) = \langle \delta z(0) \delta z(t) \rangle \quad (3)$$

where

$$\delta z(t) = z(t) - \langle z \rangle \quad (4)$$

As is obvious, an advantage of this GLE method is that the diffusion coefficient can be calculated directly from the variance of  $z$  and the correlation time  $\tau$ .

For the calculation of the diffusion coefficient profiles across the model systems, we developed a code based on the GLE method. In order to verify its validity, we performed test runs using a 1,2-dipalmitoyl-*sn*-glycero-3-phosphocholine (DPPC) PLB and we calculated the diffusion rate profile of water ( $H_2O$ ) across this system, to compare with the profiles available in literature, where DPPC PLB was also used. From figure 3 we can conclude that the obtained result is in line with the results given in literature [64, 66].

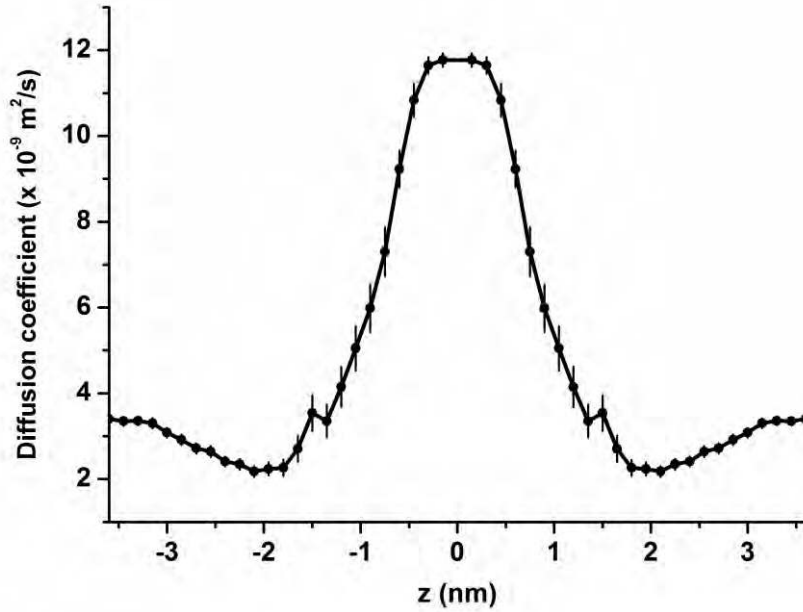


**Figure 3.** Diffusion rate profile of  $H_2O$  across a DPPC bilayer system ( $T=300$  K). The diffusion coefficient of  $H_2O$  in the water layer (i.e.,  $|z| > 3$  nm) corresponds very well to the diffusion coefficient of SPC water in a bulk water system (i.e.,  $3.6 \times 10^{-9} \text{ m}^2/\text{s}$  [58]).

Thus, using the GLE method we calculated the diffusion rate profiles, and by averaging over 24 (in the case of the AQP1 pores) and 30 (in the case of the POPC PLB) individual diffusion rate profiles, we obtained the final diffusion rate profiles of  $H_2O_2$  across each model system. Note that each diffusion rate profile was calculated using the data from the last 2ns of the US MD simulations, like for the free energy profile calculation (see previous section).

### 2.3 Permeability coefficient

Knowing the free energy (or potential of mean force  $w(z)$ ) and the diffusion coefficient ( $D(z)$ ) of a molecule solute along the  $z$ -axis of the model system, the permeability coefficient ( $P_m$ ) can be expressed as an integral over an interval of  $z$  that spans the structure [66, 67]:

$$\frac{1}{P_m} = \int_{z_1}^{z_2} \frac{e^{w(z)/k_B T}}{D(z)} dz \quad (5)$$

### 3. Results and discussion

Figure 4 illustrates the average free energy ( $\Delta G$ ) and diffusion rate profiles of  $H_2O_2$  through AQP1 and the POPC bilayer. Details about the constriction regions, i.e., Asn-Pro-Ala (NPA) and aromatic/Arg (ar/R) motifs in AQP1 (see figure 4(a,b)) providing selectivity against passage of solutes [52, 53], are given in the previous section. In figure 4(a) we applied a trapezoidal correction to the free energy profile, which allows us to directly compare the profile for AQP1 with the profile shown in figure 4(c) for the PLB. More details about the trapezoidal correction are given in [33]. Note that the profiles given in figure 4(c,d) are symmetrized (due to the bilayer symmetry), although we obtained almost the same profiles in the asymmetric cases (see figure 5).

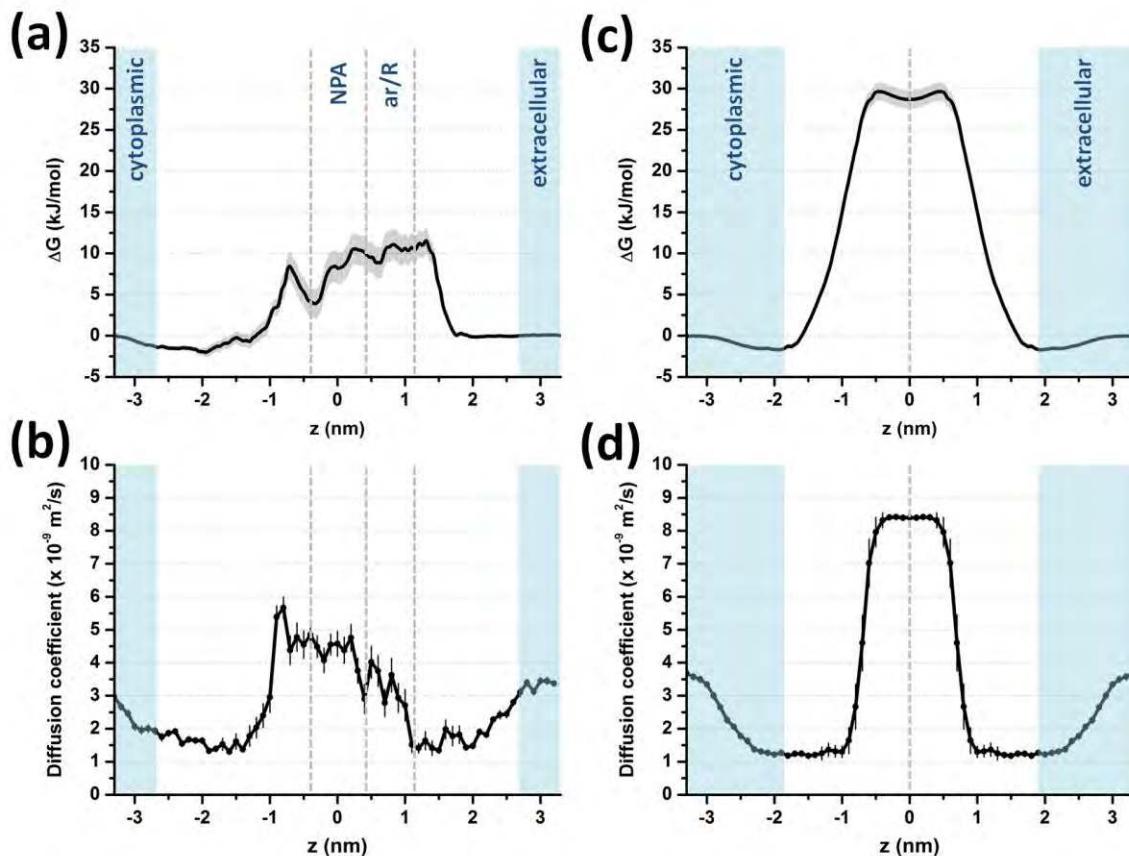


**Figure 4.** Average free energy and diffusion rate profiles of  $H_2O_2$  across AQP1 pores (a,b) and the POPC PLB (c,d). The NPA and ar/R regions in (a) and (b) are shown within the gray dashed lines. The center of the POPC bilayer in (c) and (d) corresponds to  $z=0$  nm and is indicated with a gray dashed line. The cytoplasmic and extracellular water layers are shown in light blue color. Associated standard deviations of the profiles are shown in gray (a,c) and black (b,d) colors.

The free energy profile for the POPC PLB shown in figure 4(c) corresponds very well to previously calculated profiles [33, 54], whereas the profile for AQP1 presented in figure 4(a) is somewhat lower than the profile given in [33]. This is probably attributed to the different calculation time used in this and previous calculations, or most likely because of the long range dispersion correction applied in previous simulations for energy and pressure, which is not the case in these simulations. This dispersion correction most probably does not affect the systems with lipid molecules (cf. figure 4(c) and [54]) and only has some effect on the protein systems. Nevertheless, since our aim in this study is to determine the relative permeation and find out through which of these model systems the  $H_2O_2$  molecules translocate more easily to the cell interior, we can use these results in our permeability coefficient calculations. We estimated that

the relative difference in energy values (i.e., difference between previously calculated energy profile [33] and the energy profile given in figure 4(a)) does not affect the relative permeation, as the permeability coefficient of  $\text{H}_2\text{O}_2$  through AQP1 is much greater than that across the PLB (see below).

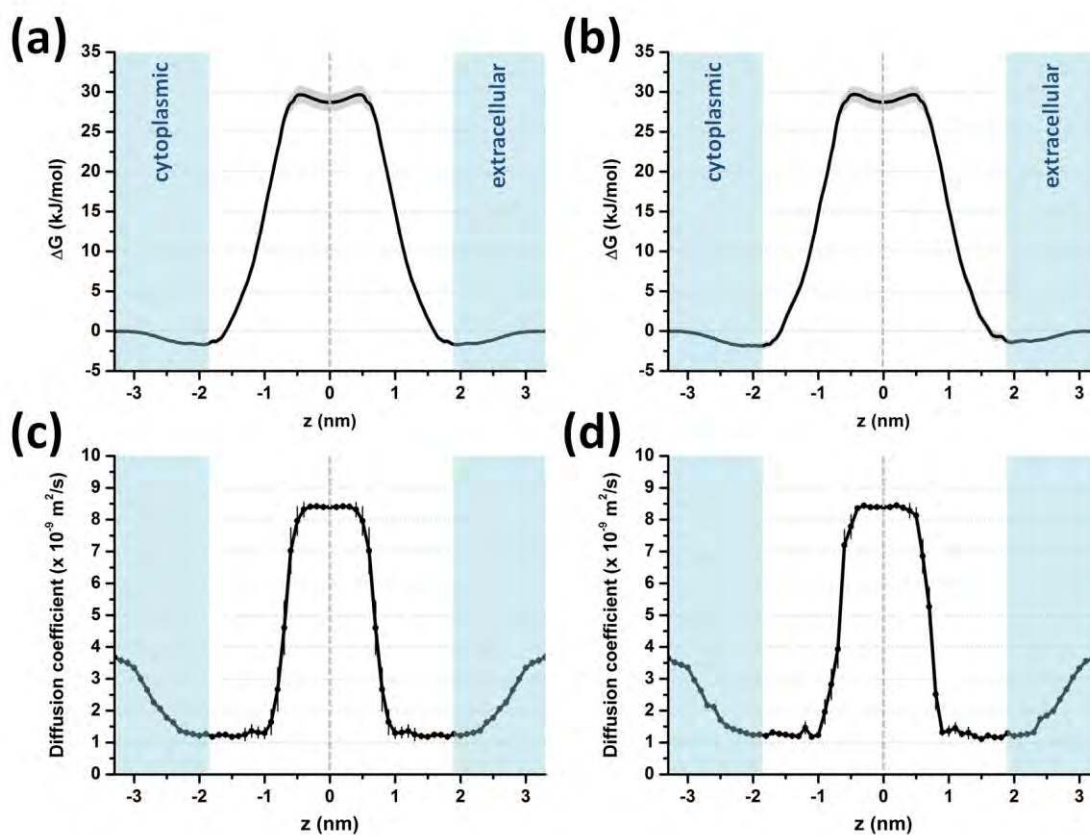


**Figure 5.** Symmetrized (a, c) and unsymmetrized (b, d) free energy and diffusion rate profiles of  $\text{H}_2\text{O}_2$  across POPC PLB. As is clear, they are almost the same (cf. (a) and (b) as well as (c) and (d)). This indicates that the performed simulations are adequate. Note that the standard deviations of the profiles are shown in gray (a,b) and black (c,d) colors.

$\text{H}_2\text{O}_2$  can, in principle, also penetrate through the central cavity of AQP1 (cf. figure 1(a)). However, we do not consider this, as the corresponding free energy barrier is much higher than through the pores (see figure 6).

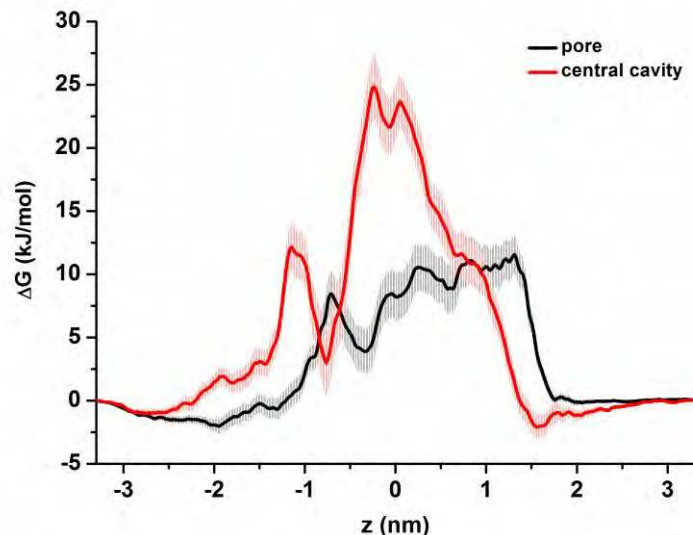


**Figure 6.** Free energy profiles of  $H_2O_2$  across AQP1 pores and the central cavity (cf. figure 1(a)). Note that the trapezoidal correction (see [33]) is not applied to these profiles, as the comparison with the  $H_2O_2$  profile through the PLB system is not performed here. The standard deviations of the profiles are shown in light red and gray colors.

It is clear from figure 4 that the free energy barrier for  $H_2O_2$  transport through AQP1 is ca. 3 times lower than through the POPC bilayer (see figure 4(a) and 4(c)), which means that the probability of  $H_2O_2$  transport across AQP1 is much higher. The reason for the lower free energy barrier of  $H_2O_2$  across AQP1 is the following. In the absence of a protein channel, the permeation of  $H_2O_2$  through the PLB follows the solubility-diffusion model [67, 68]. The excess free energy steeply increases, since  $H_2O_2$  partitions from the aqueous phase to the membrane interior, thereby losing its hydration waters. Once inside the hydrophobic core,  $H_2O_2$  diffuses in a nearly flat energy landscape (see figure 4(c)). The presence of AQP creates a more favorable pathway for  $H_2O_2$  permeation, with a significantly lower free energy barrier. This can be explained by looking at the general mechanism of water permeation through AQPs [52, 53, 69]. It is well known that AQP pores are lined by hydrophilic amino acid carbonyl groups and side chains, which allow for the formation of a narrow water file. The motion of water molecules through the pore is highly correlated. Water molecules move collectively and, under the action of the electric macrodipoles of AQPs, they change orientation as they pass through the NPA region at the pore center (cf. figure 4(a)). Earlier MD simulations have revealed that  $H_2O_2$  and small oxy-radicals remain partially hydrated as they permeate through AQPs, meaning that they do not disrupt the water file [33]. Moreover, they respond in a similar fashion as water to the electric macrodipoles. The structural similarity between  $H_2O_2$  and water reflects itself in similar permeation mechanisms that in turn explain why  $H_2O_2$  permeation is also facilitated by the AQP homolog investigated here.

The maximum diffusion coefficient of  $H_2O_2$  through AQP1 is around 1.5 times lower than through the PLB (see figure 4(b) and 4(d)), but the diffusion coefficient profile gives information about the motion ability of molecules at each  $z$  position of the system, whereas the free energy profile reveals the penetration ability to each  $z$  position from a certain position (e.g., from the water layer), showing its barrier. Therefore, comparing the energy barriers is more important than comparing the diffusion coefficients. The diffusion coefficient at each  $z$  position simply indicates whether  $H_2O_2$  moves in this position with higher or lower velocity, where reaching this position depends on the energy barrier. However, the diffusion rate profile is necessary for calculating the permeability coefficient of the solute (see eq. 5).

The calculated permeability coefficients of  $H_2O_2$  across AQP1 and the POPC bilayer show that the permeability of  $H_2O_2$  through AQP1 is at least two orders of magnitude higher than

through the POPC PLB, i.e.,  $P_{\text{AQP1}}=2.57$  cm/s and  $P_{\text{POPC PLB}}=6.62\times 10^{-3}$  cm/s. Thus, to summarize,  $\text{H}_2\text{O}_2$  most probably travels through AQPs to the cytoplasm rather than through the PLB.

We should mention here that the cell membrane on its own is a complex system consisting of different types of PLs, AQPs, etc., and we cannot take all these components into account in our simulations. Moreover, we limited ourselves by showing the results only for AQP1 and a POPC PLB, mainly due to the computational cost and time of the simulations (see section 2). However, based on the following considerations, we believe that we can still make the above mentioned conclusion. The AQP1 we chose is a typical AQP with a pore size of 2.8–3 Å [32, 49, 53], through which  $\text{H}_2\text{O}_2$  molecules with diameter 2.5–2.8 Å are able to pass [32, 50, 70]. On the other hand, some AQPs, such as AQP8 and/or aquaglyceroporins (i.e., permeated by water plus glycerol) have even bigger pore sizes, i.e., 3.2 and 3.4–4 Å, respectively [49, 71, 72], which makes the transport of  $\text{H}_2\text{O}_2$  much easier across these channels compared to other AQPs. Accordingly, the permeability coefficient of  $\text{H}_2\text{O}_2$  will also be bigger in these AQPs. In the case of the POPC, we might choose other PLBs, however, most of these systems have similar free energy profiles for the transport of  $\text{H}_2\text{O}_2$  (see e.g., [25, 27, 54]). We can expect that the  $\text{H}_2\text{O}_2$  diffusion rate profiles through these systems will also be at the same order, as these PLB systems only differ with their lipid tail compositions, having the same head groups. Hence, we can assume that the permeability coefficient of  $\text{H}_2\text{O}_2$ , which depends on the free energy and diffusion rate profiles (see eq. 5), will also be in the same order. Thus, based on these considerations, we may conclude that the permeability of  $\text{H}_2\text{O}_2$  through AQPs is at least two orders of magnitude higher than through the PLB.

In our previous studies [24–26] we showed the ability of ROS transport through the membrane upon oxidation of lipids and/or strong electric fields. The conditions of these studies in experiments most probably correspond to longer CAP treatment times or to higher plasma doses, as well as to some CAP sources which generate strong electric fields, like DBD or linear-field plasma jets. The condition of the present study most likely corresponds to lower plasma doses or short treatment times, and when the effect of electric field is excluded or negligible, i.e., where the creation of membrane pores, due to strong electric fields and/or lipid oxidation, does not occur. In practice, we thus believe that both mechanisms, i.e., transport through membrane pores and through AQP, can occur, depending on the conditions.

## 4. Conclusions

The aim of our study was to elucidate the selective anti-cancer mechanism of CAP based on the presence of AQPs in the cell membrane and to determine the precise role of AQPs in this selective anti-cancer capacity, applying computer simulations.

We studied the permeation processes of  $\text{H}_2\text{O}_2$  through AQP1 and the POPC PLB, showing that the free energy barrier for  $\text{H}_2\text{O}_2$  transport through AQP1 is ca. 3 times lower than through the POPC bilayer, and the permeability coefficient of  $\text{H}_2\text{O}_2$  is at least two orders of magnitude higher. This indicates that the AQP transmembrane proteins are the most favorable channels for  $\text{H}_2\text{O}_2$  penetration into the cell interior, rather than the PLB itself. Hence, the performed simulations give insight into the mechanisms of  $\text{H}_2\text{O}_2$  (one of the ROS) permeation into the cytoplasm. This might explain the experimentally observed faster consumption of extracellular  $\text{H}_2\text{O}_2$  by cancer cells than by normal cells, which is due to a higher expression of AQPs in cancer cells compared to homologous normal cells.

Thus, the present investigation confirms that the mechanism for the CAP treatment selectivity towards cancer cells can be explained based on a higher AQP expression in their cell membrane.

It should be mentioned that although the results of free energy profiles of some RONS through AQPs are available in literature [33, 73], the overall nature of RONS permeation across both native and RONS-modified (i.e., oxidized/nitrosated) AQPs, namely their free energy and

diffusion rate profiles as well as permeability coefficients, is still unclear. This will be the subject of our future study.

## Acknowledgements

M.Y. gratefully acknowledges financial support from the Research Foundation – Flanders (FWO), grant number 1200216N, and for obtaining a travel grant to George Washington University (GWU). The computational work was carried out using the Turing HPC infrastructure at the CalcUA core facility of the Universiteit Antwerpen (UA), a division of the Flemish Supercomputer Center VSC, funded by the Hercules Foundation, the Flemish Government (department EWI) and the UA. Work at GWU was supported by the National Science Foundation, grant 1465061. R.M.C. thanks FAPESP and CNPq for financial support (grants 2012/50680-5 and 459270/2014-1, respectively).

## References

- [1] Keidar M, Walk R, Shashurin A, Srinivasan P, Sandler A, Dasgupta S, Ravi R, Guerrero-Preston R and Trink B 2011 Cold plasma selectivity and the possibility of a paradigm shift in cancer therapy *British journal of cancer* **105** 1295
- [2] Szili E J, Hong S-H, Oh J-S, Gaur N and Short R D Tracking the Penetration of Plasma Reactive Species in Tissue Models *Trends in Biotechnology*
- [3] Yan D, Sherman J H and Keidar M 2017 Cold atmospheric plasma, a novel promising anti-cancer treatment modality *Oncotarget* **8** 15977-95
- [4] Vermeulen S, De Waele J, Vanuytsel S, De Backer J, Van der Paal J, Ramakers M, Leyssens K, Marcq E, Van Audenaerde J and LJ Smits E 2016 Cold atmospheric plasma treatment of melanoma and glioblastoma cancer cells *Plasma Processes and Polymers* **13** 1195-205
- [5] Wende K, Bekeschus S, Schmidt A, Jatsch L, Hasse S, Weltmann K, Masur K and von Woedtke T 2016 Risk assessment of a cold argon plasma jet in respect to its mutagenicity *Mutation Research/Genetic Toxicology and Environmental Mutagenesis* **798** 48-54
- [6] Yan D, Talbot A, Nourmohammadi N, Sherman J H, Cheng X and Keidar M 2015 Toward understanding the selective anticancer capacity of cold atmospheric plasma—A model based on aquaporins *Biointerphases* **10** 040801
- [7] Lin A, Truong B, Patel S, Kaushik N, Choi E H, Fridman G, Fridman A and Miller V 2017 Nanosecond-Pulsed DBD Plasma-Generated Reactive Oxygen Species Trigger Immunogenic Cell Death in A549 Lung Carcinoma Cells through Intracellular Oxidative Stress *International journal of molecular sciences* **18** 966
- [8] Kaushik N, Kim M-J, Kim R-K, Kaushik N K, Seong K M, Nam S-Y and Lee S-J 2017 Low-dose radiation decreases tumor progression via the inhibition of the JAK1/STAT3 signaling axis in breast cancer cell lines *Scientific Reports* **7** 43361
- [9] Van Boxem W, Van der Paal J, Gorbanev Y, Vanuytsel S, Smits E, Dewilde S and Bogaerts A 2017 Anti-cancer capacity of plasma-treated PBS: effect of chemical composition on cancer cell cytotoxicity *Scientific reports* **7** 16478
- [10] Canal C, Fontelo R, Hamouda I, Guillem-Marti J, Cvelbar U and Ginebra M-P 2017 Plasma-induced selectivity in bone cancer cells death *Free radical biology and medicine* **110** 72-80
- [11] Keidar M, Yan D, Beilis I I, Trink B and Sherman J H 2017 Plasmas for treating cancer: opportunities for adaptive and self-adaptive approaches *Trends in biotechnology*
- [12] Georgescu N and Lupu A R 2010 Tumoral and normal cells treatment with high-voltage pulsed cold atmospheric plasma jets *IEEE Transactions on Plasma Science* **38** 1949-55
- [13] Kim J Y, Kim S-O, Wei Y and Li J 2010 A flexible cold microplasma jet using biocompatible dielectric tubes for cancer therapy *Applied Physics Letters* **96** 203701

- [14] Zirnheld J L, Zucker S N, DiSanto T M, Berezney R and Etemadi K 2010 Nonthermal plasma needle: development and targeting of melanoma cells *IEEE Transactions on Plasma Science* **38** 948-52
- [15] Ja Kim S, Min Joh H and Chung T 2013 Production of intracellular reactive oxygen species and change of cell viability induced by atmospheric pressure plasma in normal and cancer cells *Applied Physics Letters* **103** 153705
- [16] Ishaq M, Evans M D and Ostrikov K K 2014 Atmospheric pressure gas plasma-induced colorectal cancer cell death is mediated by Nox2–ASK1 apoptosis pathways and oxidative stress is mitigated by Srx–Nrf2 anti-oxidant system *Biochimica et Biophysica Acta (BBA)-Molecular Cell Research* **1843** 2827-37
- [17] Kaushik N K, Kaushik N, Park D and Choi E H 2014 Altered antioxidant system stimulates dielectric barrier discharge plasma-induced cell death for solid tumor cell treatment *PloS one* **9** e103349
- [18] Ishaq M, Kumar S, Varinli H, Han Z J, Rider A E, Evans M D, Murphy A B and Ostrikov K 2014 Atmospheric gas plasma–induced ROS production activates TNF-ASK1 pathway for the induction of melanoma cancer cell apoptosis *Molecular biology of the cell* **25** 1523-31
- [19] Kim S J and Chung T 2016 Cold atmospheric plasma jet-generated RONS and their selective effects on normal and carcinoma cells *Scientific reports* **6** 20332
- [20] Graves D B 2012 The emerging role of reactive oxygen and nitrogen species in redox biology and some implications for plasma applications to medicine and biology *Journal of Physics D: Applied Physics* **45** 263001
- [21] Keidar M 2015 Plasma for cancer treatment *Plasma Sources Science and Technology* **24** 033001
- [22] Trachootham D, Alexandre J and Huang P 2009 Targeting cancer cells by ROS-mediated mechanisms: a radical therapeutic approach? *Nature reviews. Drug discovery* **8** 579
- [23] Cairns R A, Harris I S and Mak T W 2011 Regulation of cancer cell metabolism *Nature Reviews Cancer* **11** 85-95
- [24] Yusupov M, Wende K, Kupsch S, Neyts E, Reuter S and Bogaerts A 2017 Effect of head group and lipid tail oxidation in the cell membrane revealed through integrated simulations and experiments *Scientific Reports* **7** 5761
- [25] Yusupov M, Van der Paal J, Neyts E and Bogaerts A 2017 Synergistic effect of electric field and lipid oxidation on the permeability of cell membranes *Biochimica et Biophysica Acta (BBA)-General Subjects* **1861** 839-47
- [26] Van der Paal J, Neyts E C, Verlact C C and Bogaerts A 2016 Effect of lipid peroxidation on membrane permeability of cancer and normal cells subjected to oxidative stress *Chemical Science* **7** 489-98
- [27] Van der Paal J, Verheyen C, Neyts E C and Bogaerts A 2017 Hampering Effect of Cholesterol on the Permeation of Reactive Oxygen Species through Phospholipids Bilayer: Possible Explanation for Plasma Cancer Selectivity *Scientific reports* **7** 39526
- [28] Neto A J and Cordeiro R M 2016 Molecular simulations of the effects of phospholipid and cholesterol peroxidation on lipid membrane properties *Biochimica et Biophysica Acta (BBA)-Biomembranes* **1858** 2191-8
- [29] Shinitzky M 1984 Membrane fluidity in malignancy adversative and recuperative *Biochimica et Biophysica Acta (BBA)-Reviews on Cancer* **738** 251-61
- [30] Papadopoulos M C and Saadoun S 2015 Key roles of aquaporins in tumor biology *Biochimica et Biophysica Acta (BBA)-Biomembranes* **1848** 2576-83
- [31] Agre P, King L S, Yasui M, Guggino W B, Ottersen O P, Fujiyoshi Y, Engel A and Nielsen S 2002 Aquaporin water channels—from atomic structure to clinical medicine *The Journal of physiology* **542** 3-16
- [32] Bienert G P, Schjoerring J K and Jahn T P 2006 Membrane transport of hydrogen peroxide *Biochimica et Biophysica Acta (BBA)-Biomembranes* **1758** 994-1003

- [33] Cordeiro R M 2015 Molecular dynamics simulations of the transport of reactive oxygen species by mammalian and plant aquaporins *Biochimica et Biophysica Acta (BBA)-General Subjects* **1850** 1786-94
- [34] Ikeda M, Beitz E, Kozono D, Guggino W B, Agre P and Yasui M 2002 Characterization of aquaporin-6 as a nitrate channel in mammalian cells requirement of pore-lining residue threonine 63 *Journal of Biological Chemistry* **277** 39873-9
- [35] Herrera M, Hong N J and Garvin J L 2006 Aquaporin-1 transports NO across cell membranes *Hypertension* **48** 157-64
- [36] Nozik-Grayck E, Suliman H B and Piantadosi C A 2005 Extracellular superoxide dismutase *The international journal of biochemistry & cell biology* **37** 2466-71
- [37] Ameziane-El-Hassani R, Schlumberger M and Dupuy C 2016 NADPH oxidases: new actors in thyroid cancer? *Nature Reviews Endocrinology* **12** 485-94
- [38] Adachi T, Tanaka H, Nonomura S, Hara H, Kondo S-i and Hori M 2015 Plasma-activated medium induces A549 cell injury via a spiral apoptotic cascade involving the mitochondrial–nuclear network *Free Radical Biology and Medicine* **79** 28-44
- [39] Yan D, Nourmohammadi N, Bian K, Murad F, Sherman J H and Keidar M 2016 Stabilizing the cold plasma-stimulated medium by regulating medium's composition *Scientific reports* **6** 26016
- [40] Yan D, Cui H, Zhu W, Nourmohammadi N, Milberg J, Zhang L G, Sherman J H and Keidar M 2017 The Specific Vulnerabilities of Cancer Cells to the Cold Atmospheric Plasma-Stimulated Solutions *Scientific Reports* **7** 4479
- [41] Van Boxem W, Van der Paal J, Gorbanev Y, Vanuytsel S, LJ Smits E, Dewilde S and Bogaerts A 2017 Anti - cancer capacity of plasma - treated PBS: effect of chemical composition on cancer cell cytotoxicity *Scientific reports* accepted for publication
- [42] Yan D, Talbot A, Nourmohammadi N, Cheng X, Canady J, Sherman J and Keidar M 2015 Principles of using cold atmospheric plasma stimulated media for cancer treatment *Scientific reports* **5** 18339
- [43] Tanaka H, Nakamura K, Mizuno M, Ishikawa K, Takeda K, Kajiyama H, Utsumi F, Kikkawa F and Hori M 2016 Non-thermal atmospheric pressure plasma activates lactate in Ringer's solution for anti-tumor effects *Scientific reports* **6** 36282
- [44] Girard P-M, Arbabian A, Fleury M, Bauville G, Puech V, Dutreix M and Sousa J S 2016 Synergistic effect of H<sub>2</sub>O<sub>2</sub> and NO<sub>2</sub> in cell death induced by cold atmospheric He plasma *Scientific reports* **6** 29098
- [45] Kurake N, Tanaka H, Ishikawa K, Kondo T, Sekine M, Nakamura K, Kajiyama H, Kikkawa F, Mizuno M and Hori M 2016 Cell survival of glioblastoma grown in medium containing hydrogen peroxide and/or nitrite, or in plasma-activated medium *Archives of biochemistry and biophysics* **605** 102-8
- [46] Lopez-Lázaro M 2007 Dual role of hydrogen peroxide in cancer: possible relevance to cancer chemoprevention and therapy *Cancer letters* **252** 1-8
- [47] Yan D, Xiao H, Zhu W, Nourmohammadi N, Zhang L G, Bian K and Keidar M 2017 The role of aquaporins in the anti-glioblastoma capacity of the cold plasma-stimulated medium *Journal of Physics D: Applied Physics* **50** 055401
- [48] Miller E W, Dickinson B C and Chang C J 2010 Aquaporin-3 mediates hydrogen peroxide uptake to regulate downstream intracellular signaling *Proceedings of the National Academy of Sciences* **107** 15681-6
- [49] Almasalmeh A, Krenc D, Wu B and Beitz E 2014 Structural determinants of the hydrogen peroxide permeability of aquaporins *The FEBS journal* **281** 647-56
- [50] Bienert G P and Chaumont F 2014 Aquaporin-facilitated transmembrane diffusion of hydrogen peroxide *Biochimica et Biophysica Acta (BBA)-General Subjects* **1840** 1596-604

- [51] Bienert G P, Møller A L, Kristiansen K A, Schulz A, Møller I M, Schjoerring J K and Jahn T P 2007 Specific aquaporins facilitate the diffusion of hydrogen peroxide across membranes *Journal of Biological Chemistry* **282** 1183-92
- [52] Sui H, Han B-G, Lee J K, Walian P and Jap B K 2001 Structural basis of water-specific transport through the AQP1 water channel *Nature* **414** 872-8
- [53] Murata K, Mitsuoka K, Hirai T and Walz T 2000 Structural determinants of water permeation through aquaporin-1 *Nature* **407** 599
- [54] Cordeiro R M 2014 Reactive oxygen species at phospholipid bilayers: distribution, mobility and permeation *Biochimica et Biophysica Acta (BBA)-Biomembranes* **1838** 438-44
- [55] Hoover W G 1985 Canonical dynamics: equilibrium phase-space distributions *Physical review A* **31** 1695
- [56] Parrinello M and Rahman A 1981 Polymorphic transitions in single crystals: A new molecular dynamics method *Journal of Applied physics* **52** 7182-90
- [57] Schmid N, Eichenberger A P, Choutko A, Riniker S, Winger M, Mark A E and van Gunsteren W F 2011 Definition and testing of the GROMOS force-field versions 54A7 and 54B7 *European biophysics journal* **40** 843
- [58] Berendsen H J, Postma J P, van Gunsteren W F and Hermans J 1981 *Intermolecular forces*: Springer) pp 331-42
- [59] Essmann U, Perera L, Berkowitz M L, Darden T, Lee H and Pedersen L G 1995 A smooth particle mesh Ewald method *The Journal of chemical physics* **103** 8577-93
- [60] Hess B, Kutzner C, Van Der Spoel D and Lindahl E 2008 GROMACS 4: algorithms for highly efficient, load-balanced, and scalable molecular simulation *Journal of chemical theory and computation* **4** 435-47
- [61] Van Der Spoel D, Lindahl E, Hess B, Groenhof G, Mark A E and Berendsen H J 2005 GROMACS: fast, flexible, and free *Journal of computational chemistry* **26** 1701-18
- [62] Kumar S, Rosenberg J M, Bouzida D, Swendsen R H and Kollman P A 1992 The weighted histogram analysis method for free - energy calculations on biomolecules. I. The method *Journal of computational chemistry* **13** 1011-21
- [63] Hummer G 2005 Position-dependent diffusion coefficients and free energies from Bayesian analysis of equilibrium and replica molecular dynamics simulations *New Journal of Physics* **7** 34
- [64] Awoonor-Williams E and Rowley C N 2016 Molecular simulation of nonfacilitated membrane permeation *Biochimica et Biophysica Acta (BBA)-Biomembranes* **1858** 1672-87
- [65] Allen M P and Tildesley D J 1989 *Computer simulation of liquids*: Oxford university press)
- [66] Marrink S J and Berendsen H J 1996 Permeation process of small molecules across lipid membranes studied by molecular dynamics simulations *The Journal of Physical Chemistry* **100** 16729-38
- [67] Marrink S-J and Berendsen H J 1994 Simulation of water transport through a lipid membrane *The Journal of Physical Chemistry* **98** 4155-68
- [68] Finkelstein A 1987 Water movement through lipid bilayer, pores and plasma membranes *Theory and Reality* **4**
- [69] de Groot B L and Grubmüller H 2001 Water permeation across biological membranes: mechanism and dynamics of aquaporin-1 and GlpF *Science* **294** 2353-7
- [70] Henzler T and Steudle E 2000 Transport and metabolic degradation of hydrogen peroxide in *Chara corallina*: model calculations and measurements with the pressure probe suggest transport of H<sub>2</sub>O<sub>2</sub> across water channels *Journal of experimental botany* **51** 2053-66
- [71] Beitz E, Becker D, Bülow J, Conrad C, Fricke N, Geadkaew A, Krenc D, Song J, Wree D and Wu B 2009 In vitro analysis and modification of aquaporin pore selectivity *Aquaporins* 77-92

- [72] Fu D, Libson A, Miercke L J, Weitzman C, Nollert P, Krucinski J and Stroud R M 2000 Structure of a glycerol-conducting channel and the basis for its selectivity *Science* **290** 481-6
- [73] Wang Y and Tajkhorshid E 2010 Nitric oxide conduction by the brain aquaporin AQP4 *Proteins: Structure, Function, and Bioinformatics* **78** 661-70